Inorganic Chemistry

Article

pubs.acs.org/IC

Distorted Phosphorus and Copper Square-Planar Layers in $LaCu_{1+x}P_2$ and $LaCu_4P_3$: Synthesis, Crystal Structure, and Physical Properties

Jian Wang, Kathleen Lee, and Kirill Kovnir*

Department of Chemistry, University of California—Davis (UC Davis), One Shields Avenue, Davis, California 95616, United States

Supporting Information

ABSTRACT: Two new lanthanum copper phosphides, $LaCu_{1+x}P_2$ and $LaCu_4P_3$, were synthesized from elements. Their crystal structures were determined by means of single-crystal X-ray diffraction. $LaCu_{1+x}P_2$ crystallizes in a complex crystal structure, a derivative of the $HfCuSi_2$ structure type, in the space group *Cmmm* (No. 65) with unit cell parameters of a = 5.564(3) Å, b = 19.96(1) Å, c = 5.563(3) Å, and Z = 8. Its crystal structure features disordered $Cu_{2x}P_2$ layers alternated with fully ordered PbO-like Cu_2P_2 layers. The Cu−P layers are separated by La counter-cations. The $Cu_{2x}P_2$ layers are composed of rectangular P_4 polyphosphide rings connected by partially occupied Cu atoms. Investigations of the electrical resistivity and Seebeck thermopower for $LaCu_{1+x}P_2$ reveal metallic-type behavior with holes as the main charge carriers. $LaCu_{1+x}P_2$ exhibits unexpectedly low thermal conductivity presumably because of disorder in the $Cu_{2x}P_2$ layers. $LaCu_4P_3$ crystallizes in a new structure type, in the tetragonal space group *P4/nmm* (No. 129) with unit cell parameters of a = 5.788(2) Å, c = 7.353(2) Å, and Z = 2. Its crystal structure features distorted square nets of Cu atoms within the Cu_4P_3 slabs. Electron localization function analysis indicates that both P atoms in $LaCu_4P_3$ have 1 + 4 coordination involving multicenter Cu−P bonding. According to the density of states and band structure, $LaCu_4P_3$ is predicted to be a metallic conductor.

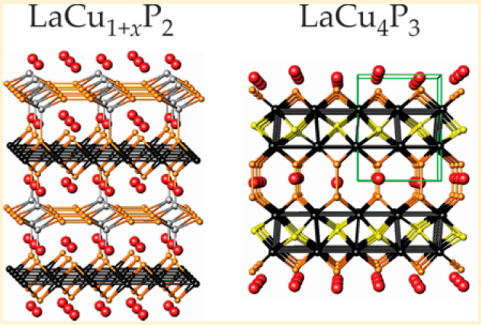

INTRODUCTION

Exploring new intermetallic compounds and rationalizing the relationships between their structures and properties were of essential interest to the solid-state chemistry community in the past decades.[1−5] Prof. John Corbett was a trendsetter in this field of research.[1] For transition-metal phosphides, several intriguing properties were observed, such as superconductivity and unconventional magnetism in $ThCr_2Si_2$-type phosphides,[6,7] high catalytic activity for CoP_3[8] and Ni_2P,[9] and remarkable Li capacity and stability during electrochemical cycling of some transition-metal phosphides.[10] Our group is searching for new phosphide-based thermoelectric materials.[11−14]

In the R−Cu−P system (R = rare-earth elements), various structural motifs have been reported[15−24] together with interesting physical phenomena such as symmetry-breaking transitions shown in $HoCuP_2$,[25] $ErCuP_2$,[25] and $SmCu_{1.15}P_2$.[26] Surprisingly, in the La−Cu−P system, only two compounds, $La_5Cu_{19}P_{12}$[17] and $LaCu_{3.7}P_2$,[19] have been reported, and only the former one was structurally characterized. Assuming that more phosphorus-rich phases should exist in this system, we performed a search for new lanthanum copper phosphides. This search resulted in the discovery of two new compounds, $LaCu_{1+x}P_2$ and $LaCu_4P_3$. The crystal and electronic structures as well as the physical properties of these compounds are reported in this work.

EXPERIMENTAL SECTION

All preparation processes were handled in an argon-filled glovebox with $p(O_2)$ < 1 ppm. All starting materials were from Alfa Aesar and were used as received: lanthanum (99.9%), copper (99.9%), red phosphorus (99%), potassium chloride (99%), and sodium chloride (99%).

Black platelike crystals of $LaCu_{1.09}P_2$ were found in the sample with a nominal composition of $LaCuP_{2.83}$. This sample was synthesized from a mixture of 6:6:11 LaP/Cu/P annealed for 1 day at 1250 K, followed by 7 days at 900 K. After the composition was established through a single-crystal experiment, a single-phase polycrystalline sample of $LaCu_{1+x}P_2$ was synthesized from elements. The elements were mixed in a ratio of 1:1:2.1 La/Cu/P, placed in a carbonized silica ampule, evacuated to a pressure of 10^{-2} mbar, and flame-sealed. The sealed ampules were heated from room temperature to 1073 K over 17 h, annealed for 24 h, and then cooled in the furnace. Samples were then ground in the glovebox, sealed under vacuum inside a carbonized silica ampule, heated to 1073 K over 17 h, and annealed again for 144 h.

A single crystal of $LaCu_4P_3$ was first found from a reaction with the molar ratio of 4:9:14:60 La/Cu/P/KCl. The reaction mixture was loaded into a silica ampule, sealed under vacuum, heated from room temperature to 773 K over 12 h, and then annealed at this temperature to homogenize for 48 h. Afterward, the reaction temperature was raised to 1073 K over 24 h, the mixture was annealed at this temperature for 168 h, and then the furnace was turned off. KCl was

Special Issue: To Honor the Memory of Prof. John D. Corbett

Received: September 12, 2014
Published: October 27, 2014

removed by washing the sample with water. Some black crystals were determined to be $LaCu_4P_3$ via single-crystal X-ray diffraction (XRD). After the composition was determined, La, Cu, and P were mixed in a stoichiometric ratio with a 120-fold molar excess of NaCl/KCl (1:1) flux and annealed with the same heating profile. According to powder XRD, $LaCu_4P_3$ was reproducibly synthesized as a mixture of $LaCu_4P_3$ and $La_5Cu_{19}P_{12}$. All of our attempts to synthesize a phase-pure sample of $LaCu_4P_3$ using different fluxes and flux-free reactions from elements, gas-transport reactions, and different temperature profiles were unsuccessful. Despite a relatively high yield of $LaCu_4P_3$ (up to 80%), all samples contained an admixture of $La_5Cu_{19}P_{12}$ = $LaCu_{3.8}P_{2.4}$.[17]

Powder XRD and Elemental Analysis. The samples were characterized by powder XRD using either a Bruker D8 Advance or a Rigaku Miniflex 600 diffractometer employing Cu Kα radiation. High-resolution synchrotron powder XRD data were collected at Beamline 11-BM at the Advanced Photon Source (APS), Argonne National Laboratory, using a wavelength of 0.413734 Å. Elemental analysis of selected single crystals was carried out on a Hitachi S4100T scanning electron microscope with energy-dispersive X-ray microanalysis (Oxford INCA Energy). Sample analyses confirmed the presence of only La, Cu, and P in the samples (Figure S2 and Table S3 in the Supporting Information, SI).

Single-Crystal XRD. Data were collected at 90 K using a Bruker AXS SMART diffractometer with an APEX-II CCD detector with Mo Kα radiation. The data set was recorded as ω scans with a 0.3° step width and integrated with the Bruker *SAINT* software package.[27] An analytical absorption correction was applied for $LaCu_4P_3$ using crystal face indexing. For the less regularly shaped crystal of $LaCu_{1+x}P_2$, the multiscan absorption correction was applied.[27] The solution and refinement of the crystal structure were carried out using the *SHELX* suite of programs.[28] The final refinement was performed using anisotropic atomic displacement parameters for all atoms. A summary of pertinent information relating to unit cell parameters, data collection, and refinements is provided in Table 1, and the atomic parameters and interatomic distances are provided in Tables S1 and S2 in the SI. Further details of the crystal structure determination may be obtained from Fachinformations-zentrum Karlsruhe, D-76344 Eggenstein-Leopoldshafen, Germany, by quoting the depository numbers CSD- 428492 ($LaCu_4P_3$) and CSD-428493 ($LaCu_{1.09}P_2$).

Table 1. Selected Crystal Data and Structure Refinement Parameters for $LaCu_{1.09}P_2$ and $LaCu_4P_3$

formula	$LaCu_{1.093(2)}P_{2.00(1)}$	$LaCu_4P_3$
fw (g/mol)	270.27	485.98
temperature (K)	90(2)	90(2)
radiation, wavelength (Å)	Mo Kα, 0.71073	Mo Kα, 0.71073
cryst syst	orthorhombic	tetragonal
space group	*Cmmm* (No. 65)	*P4/nmm* (No. 129)
unit cell dimens		
a (Å)	5.564(3)	5.788(2)
b (Å)	19.96(1)	
c (Å)	5.563(3)	7.353(2)
unit cell volume (Å^3)	617.7(6)	246.3(1)
Z	8	2
density (calcd) (g/cm^3)	5.812	6.552
abs coeff (cm^{-1})	21.86	26.26
data/param	552/41	240/18
final *R* indices[a] [$I > 2\sigma(I)$]	R1 = 0.012, wR2 = 0.027	R1 = 0.024, wR2 = 0.060
final *R* indices[a] [all data]	R1 = 0.023, wR2 = 0.032	R1 = 0.024, wR2 = 0.060
GOF	1.12	1.48
diff peak and hole [e/Å^3]	1.71 and −0.74	0.90 and −3.00

[a] $R1 = \sum||F_o| - |F_c||/\sum|F_o|$; $wR2 = [\sum[w(F_o^2 - F_c^2)^2]/\sum[w(F_o^2)^2]]^{1/2}$, where $w = 1/[\sigma^2F_o^2 + (AP)^2 + BP]$, with $P = (F_o^2 + 2F_c^2)/3$; *A* and *B* are weight coefficients; $A = 0.0114$ and $B = 2.937$ for $LaCu_{1.09}P_2$; $A = 0.0247$ and $B = 0.9012$ for $LaCu_4P_3$.

Differential Scanning Calorimetry (DSC). A Netzsch differential scanning calorimeter was used to characterize the thermal behavior of $LaCu_{1+x}P_2$. The DSC measurement was performed on 61 mg of a sample that was sealed inside an evacuated silica ampule. The sample amount was sufficient to cover the base of the ampule. The sample was heated to 1273 K and then cooled to room temperature with a heating/cooling rate of 10 K/min.

Quantum-Chemical Calculations. Calculations were performed only for the fully ordered structure of $LaCu_4P_3$. The presence of significant disorder and partial occupancies prevented calculations for $LaCu_{1+x}P_2$. The electronic structure calculations and bonding analysis were carried out using the tight-binding, linear-muffin-tin orbital, atomic sphere approximation (*TB-LMTO-ASA*) program.[29] The Barth−Hedin exchange potential was employed for the local density approximation calculations. The radial scalar-relativistic Dirac equation was solved to obtain the partial waves. A basis set containing La(6s,5d,4f), Cu(4s,4p,3d), and P(3s,3p) orbitals was employed for the self-consistent calculation, with La(6p) and P(3d) functions being downfolded. The density of states (DOS) and band structure were calculated after convergence of the total energy on a dense *k* mesh with 24 × 24 × 20 points, with 1001 irreducible *k* points. For bonding analysis, the energy contributions from all electronic states for selected atomic pairs were evaluated with crystal orbital Hamilton population (COHP) analysis.[30] Integration over all filled states yielded ICOHP values as an approximation of relative bond strengths. The electron localization function (ELF, η)[31−33] was evaluated with the modules implemented within the TB−LMTO−ASA package. The *ParaView* program was used for visualization of ELF isosurfaces.[34,35]

Sample Densification. A powdered single-phase sample of $LaCu_{1+x}P_2$ was compacted using spark plasma sintering (Dr. Sinter, Fuji Electronic Industrial Co.). A 4 mm graphite pressure die with WC plungers was used. The sample was compacted at an applied temperature of 873 K and a pressure of 156 MPa. The pressed sample was polished to remove graphite. The resulting geometrical density was 95% of the theoretical X-ray density.

Physical Properties. Transport properties in the temperature range of 2−300 K were studied using the commercial multipurpose Physical Properties Measurement System (PPMS, Quantum Design). The Seebeck thermopower and thermal conductivity were measured using the Thermal Transport Option. The electrical resistivity was measured by a standard four-point alternating-current technique to exclude the resistance of the leads.

RESULTS AND DISCUSSION

Crystal Structure of $LaCu_{1+x}P_2$. $LaCu_{1+x}P_2$ crystallizes in the layered structure similar to that of the Ce- and Sm-containing analogues. This type of crystal structure closely resembles the $HfCuSi_2$ structure type. Indexing only the strong XRD peaks in the single-crystal experiment for $LaCu_{1+x}P_2$ results in the tetragonal space group *I*4/*mmm* (No. 139) with unit cell parameters of $a = 3.933(2)$ Å and $c = 19.96(1)$ Å. However, a large number of weak but noticeable diffraction peaks, 439 out of 2896 reflections with $I > 3\sigma(I)$, indicate that the actual symmetry is lower than tetragonal. Indexing all of the diffraction peaks results in an orthorhombic symmetry with a doubling of the unit cell volume. The crystal structure was solved in the *Cmmm* space group (No. 65) with unit cell parameters of $a = 5.564(3)$ Å, $b = 19.96(1)$ Å, and $c = 5.563(3)$ Å. The difference between the calculated powder XRD patterns for both tetragonal and orthorhombic solutions is quite small. To check whether the structure is actually orthorhombic, we collected high-resolution powder XRD data using the APS Beamline 11-BM. The synchrotron powder XRD pattern indicates that the true symmetry is indeed orthorhombic (Figure 1). For example, near the main diffraction peak at 0.411

dx.doi.org/10.1021/ic502234w | *Inorg. Chem.* 2015, 54, 890−897

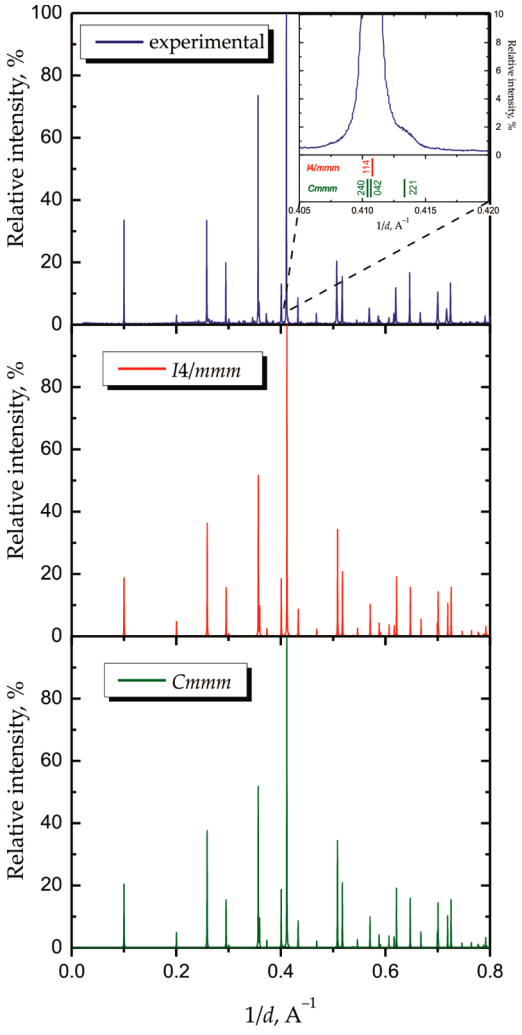

Figure 1. Experimental synchrotron powder XRD pattern (top) and calculated patterns for $LaCu_{1+x}P_2$ (below). The inset in the top panel shows the pattern enlarged around 0.41 $Å^{-1}$. Calculated peak positions are shown with red (*I4/mmm*) and green (*Cmmm*) vertical ticks. The intensity of the calculated (221) diffraction peak in the *Cmmm* model is 1%.

$Å^{-1}$, which corresponds to the (114) reflection in *I4/mmm* and two reflections (240)/(042) in *Cmmm*, there is a shoulder at 0.413 $Å^{-1}$ that is an expected (211) diffraction peak with a calculated intensity of 1% for the orthorhombic *Cmmm* structure. There is no such peak for the *I4/mmm* model (Figure 1, inset). Similar conclusions were reported for the Sm-containing analogue,[26] with an additional argument toward orthorhombic symmetry due to the loss of 4-fold rotation in the P layer, which was also observed for $LaCu_{1+x}P_2$ (vide infra).

In the crystal structure of $LaCu_{1+x}P_2$, the PbO-like Cu_2P_2 layers alternate with $Cu_{2x}P_2$ layers that have a structure derived from a square net of P atoms (Figures 2 and 3). La^{3+} cations are sandwiched between Cu−P layers. The Cu_2P_2 and La layers are fully ordered. However, the Cu2 atomic sites within the $Cu_{2x}P_2$ layer are only partially occupied, sof = 18.6(4)%. The P position in this layer splits into three positions with partial occupancies: P3a, P3b, and P3c. Unconstrained refinement of the occupancies of these atomic positions with the atomic displacement parameters set to be equal results in a total occupancy of 1.00(1). The refined composition of the compound is $LaCu_{1.093(2)}P_{2.00(1)}$.

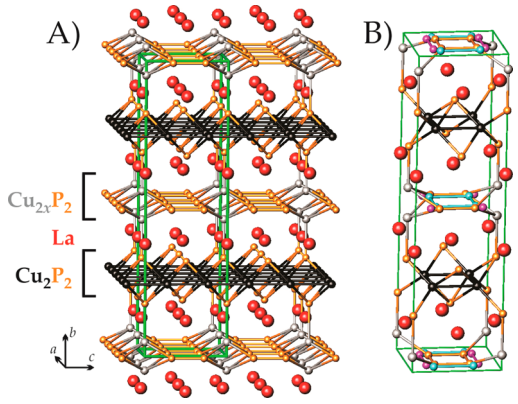

Figure 2. Crystal structure of $LaCu_{1+x}P_2$: (A) general view; (B) unit cell content. Color code: La, red; Cu1, black; Cu2, gray; P, orange, cyan, and purple. In part A, the P3b (cyan) and P3c (purple) atoms are omitted for clarity.

In the P layer, only one out of three P atoms may be present in each position because of unreasonably short distances between the P3a, P3b, and P3c atoms (Figure 3). In addition, the Cu2−Cu2 distance, 1.91(1) Å, is too short for a Cu−Cu bond. The Cu2−P3a distance, 2.56 Å, lies between the Cu2−P2 distances of 2.60 Å and the Cu1−P1 and Cu1−P2 distance of 2.43 Å. Distances between Cu2 and P3b or P3c are significantly shorter, 2.16 and 2.17 Å, respectively, which is outside the range of typical Cu−P distances.[36] Taking into account the occupancies of the atomic positions, we propose three simple possibilities for the ordering of Cu and P atoms in this layer (Figure 3B−D). The Cu2 and P3a atoms form a layer with almost square P_4 rings connected by Cu atoms. Similar square P_4 fragments connected by transition-metal atoms are present in $BaNi_2P_4$,[37] skutterudites MP_3,[38] and AM_4P_{12} (M = Fe, Co; A = alkaline, alkali-earth, and rare-earth cations).[38] In turn, P3b and P3c atoms form planar Cu-free layers with slightly longer P−P distances within the rectangular P_4 units. P−P distances of 2.2−2.3 Å are typical for covalent P bonds.[13,39] Longer P−P distances are less common but have been observed in some polyphosphides, such as CeP_2,[40] $Ba_8Cu_{16}P_{30}$,[41] and BaP_8.[42] The crystal structure of $LaCu_{1+x}P_2$ can be described as a stacking of fully occupied and ordered Cu_2P_2 layers (Figure 3F) and partially occupied $Cu_{2x}P_2$ or P_2 layers along the *b* axis (Figure 3B−E).

The shortest La−P interatomic distances vary from 2.92−2.94 Å (La1−P3c and La2−P3b) to 3.01−3.02 Å (La−P1 and La−P2). The La−P3a distance is longer, 3.12 Å. The La−P distance of ∼2.9 Å is shorter than the corresponding distances in $La_5Cu_{19}P_{12}$ (from 3.0 to 3.1 Å)[17] but similar to those found in LaP_2,[43] LaNiP,[44] and $La_3Zn_2P_4$.[45]

Crystal Structure of $LaCu_4P_3$. $LaCu_4P_3$ crystallizes in the tetragonal space group *P4/nmm* (No. 129) with unit cell parameters of *a* = 5.788(2) Å and *c* = 7.353(2) Å. The crystal structure of $LaCu_4P_3$ can also be derived using the basic PbO-like Cu_2P_2 layers (Figure 4). Condensing two layers yields a double layer with the composition Cu_4P_3 (Figure 4B). The Cu_4P_3 slabs are separated by layers of La atoms, resulting in an overall composition of $LaCu_4P_3$. The La atoms are coordinated by 8P and 8Cu atoms. The interatomic La−P distances are in the range of 3.06−3.16 Å, which are similar to La−P distances in $La_5Cu_{19}P_{12}$.[17]

There are several phosphides and sulfides with a 1−4−3 composition, such as KCu_4S_3,[46] $RbZn_4P_3$,[47] and $EuCu_4P_3$,[48]

dx.doi.org/10.1021/ic502234w | Inorg. Chem. 2015, 54, 890−897

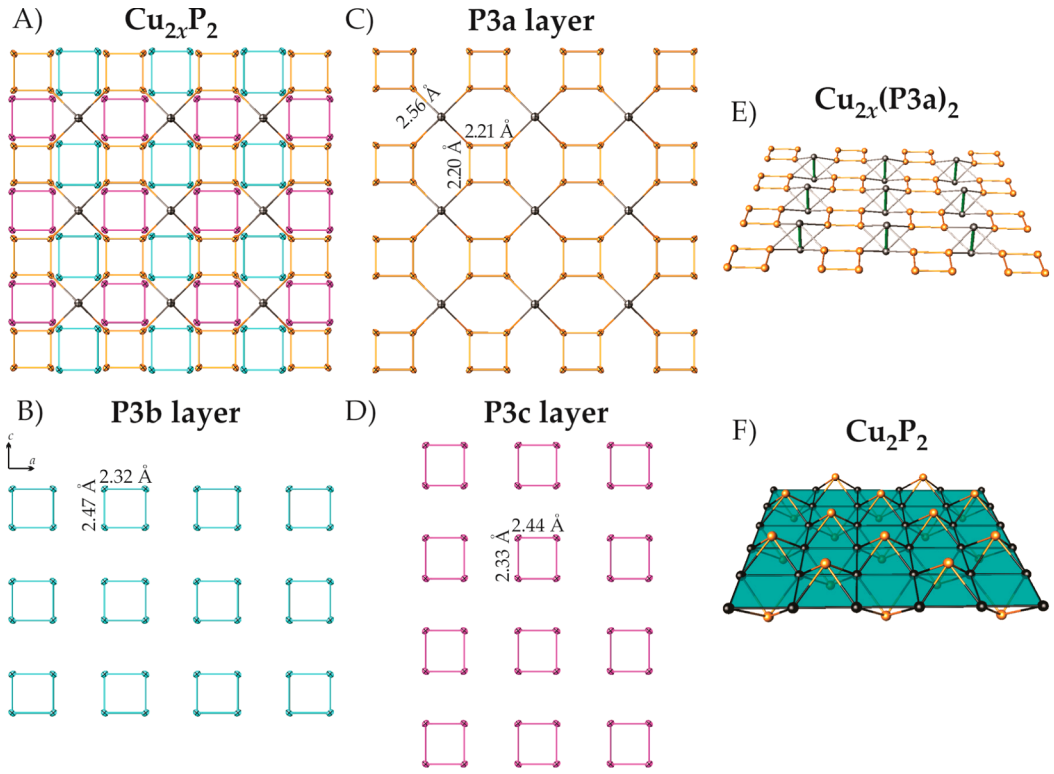

Figure 3. Structure of the $Cu_{2x}P_2$ layer: view along [010] showing (A) all atoms, (B) P3b atoms, (C) Cu2 and P3a atoms, and (D) P3c atoms. (E) Side view of the $Cu_{2x}P_2$ layer with short Cu−Cu distances shown by green lines that are physically impossible. Color code: Cu2, gray; P3a, orange; P3b, cyan; P3c, purple. (F) Side view of the fully ordered Cu_2P_2 layer. Color code: Cu1, black; P1 and P2, orange.

with crystal structures derived from the condensation of M_2P_2 PbO-like layers. All of these compounds crystallize in the tetragonal *P*4/*mmm* (No. 123) space group. In turn, $LaCu_4P_3$ crystallizes in a new structure type, in the space group *P*4/*nmm* (No. 129). Replacement of the mirror plane with an *n*-glide plane is due to significant distortion of the square Cu layer (Figure 4D). In the aforementioned $LaCu_{1+x}P_2$ crystal structure, the square P layer was distorted into isolated P_4 squares and rectangles. In the crystal structure of $LaCu_4P_3$, the planar Cu layer is distorted into Cu_4 squares with short and long Cu−Cu distances of 2.69 and 3.09 Å (Figure 4D). Distortion of the Cu layer results in a significant alteration of the coordination of the P2 atoms inside the Cu_4P_3 slab (Figure 4C). In $EuCu_4P_3$ [*P*4/*mmm* (No. 123)], similar P atoms are surrounded by Cu_8 square prisms (4/*mmm* local symmetry) with eight equivalent Cu−P distances of 2.41 Å.[48] In $LaCu_4P_3$, the P2 atom is surrounded by a Cu_8 trapezoidal prism (4*mm* local symmetry) with four short (2.39 Å) and four long (2.44 Å) Cu−P distances.

Dumbbells of P1 atoms, *d*(P1−P1) = 2.26 Å, connect the Cu_4P_3 slabs (Figure 4). P1 has a tetragonal-pyramidal coordination of one P atom and four Cu atoms at a distance of 2.42 Å. These distances are typical for P−P[13,39] and Cu−P bonds in CuP_2, Cu_2P_7, and ternary Cu-containing polyphosphides.[49]

Because of the presence of P−P bonds, both $LaCu_4P_3$ and $EuCu_4P_3$[48] are not layered but are 3D framework compounds. This differentiates them from alkaline-metal analogues, KCu_4S_3[46] and $RbZn_4P_3$,[47] which are truly 2D compounds with interlayer distances exceeding 4 Å. To get a deeper understanding of the bonding in $LaCu_4P_3$, we analyzed the electronic structure.

Band Structure of $LaCu_4P_3$. Assigning a formal charge of 1+ to the Cu atoms results in the charge-balanced formula $La^{3+}(Cu^{+})_4(P_2^{4-})P^{3-}$. However, according to calculations, $LaCu_4P_3$ has no band gap and metallic properties are expected (Figure 5). The Fermi level is located in the pseudogap. The highest contribution to the state below the Fermi level is from Cu(3d) orbitals, with some contributions from the P(3p) and La(5d) orbitals. The empty states above the Fermi level are comprised of the La(5d), La(4f), Cu(4s), and P(3p) orbitals.

P1−P1 interactions have antibonding character near the Fermi level, but overall the ICOHP value is the highest among all interatomic interactions in this crystal structure, indicating strong covalent bonding between P1 atoms (Figure 6A). Similar results were observed for $BaAu_2P_4$[12] and Au_2PbP_2.[50] All three types of Cu−P interactions exhibit similar bonding character, with slightly smaller values for longer Cu2−P distances, 1.85 versus 1.94−1.96 (Figure 6B). Tiny differences are visible in the inset: Cu−P1 interactions have essentially nonbonding character below the Fermi level and antibonding character above the Fermi level; Cu−P2 interactions at a shorter distance of 2.39 Å have weak bonding character below and above the Fermi level, while Cu−P2 interactions at a longer distance of 2.44 Å have bonding character below the Fermi level and nonbonding character above the Fermi level. COHP calculations show that there are weak Cu−Cu interactions along the shortest distance of 2.55 Å (Figure 6C). Longer Cu−Cu interactions have pronounced nonbonding and antibonding character and small ICOHP values, indicating that those long Cu−Cu distances do not correspond to chemical bonds. Interatomic interactions were additionally analyzed by means of the ELF formalism.

dx.doi.org/10.1021/ic502234w | *Inorg. Chem.* 2015, 54, 890−897

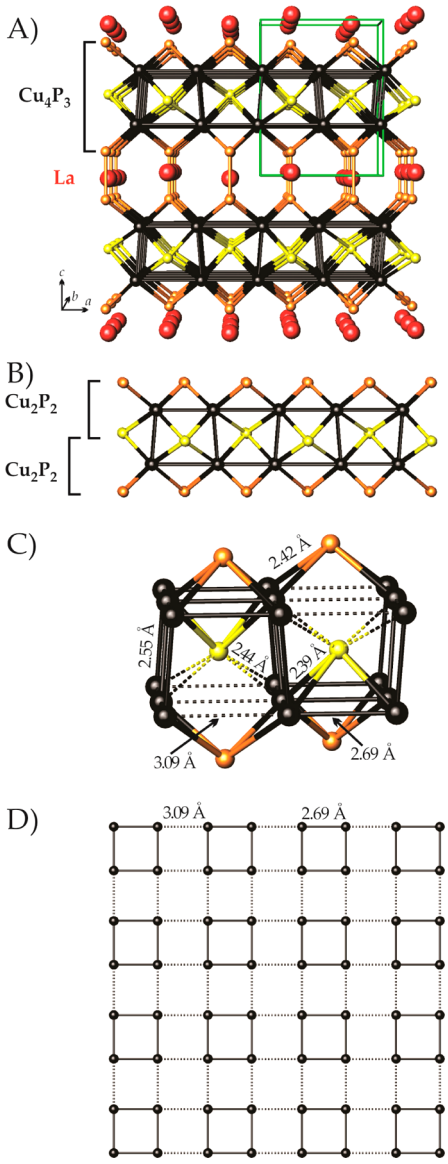

Figure 4. Crystal structure of $LaCu_4P_3$: (A) general view with the unit cell shown in green; (B) two condensed Cu_2P_2 PbO-like layers forming a Cu_4P_3 layer; (C) local coordination of P2 atoms; (D) planar layer of copper atoms. Color code: La, red; Cu, black; P1, orange; P2, yellow.

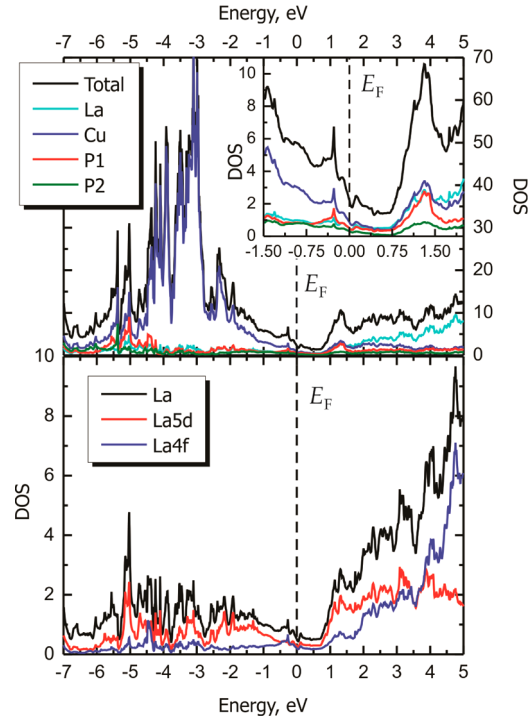

Figure 5. DOS diagrams for $LaCu_4P_3$. In the top panel, the contributions from La, Cu, and the two types of P atoms are shown in cyan, blue, red, and green, respectively. The contributions of Cu(3d) and P(3p) orbitals dominate the Cu and P atomic contributions. The inset shows an enlarged portion around the Fermi level. The bottom panel shows the orbital contributions of La(5d) and La(4f).

ELF analysis reveals several important bonding features. An attractor corresponding to the P1−P1 covalent bond is clearly visible in Figure 7A−C. P1 atoms do not form four additional covalent Cu−P bonds; instead the torus-like ELF distribution indicates multicenter Cu−P interactions. The two maxima of this distribution are shown in Figure 7B. The coordination of P1 can be described as a two-center two-electron P−P bond plus one multicenter 1P−4Cu interaction. A similar type of bonding is found in $ThCr_2Si_2$-type phosphides with short interlayer separation.[51]

Interestingly, P2 atoms have bonding characteristics similar to those of P1 atoms despite the quite different coordination. P2 forms a multicenter bond with four Cu atoms at a shorter distance of 2.39 Å (Figure 7F) and has an electron lone pair pointed toward the other four Cu atoms at longer distances of 2.44 Å (Figure 7D−F). This is a typical coordination of P atoms in the $ThCr_2Si_2$-type phosphides with long interlayer separation.[51] Thus, both P atoms have 1 + 4 coordination: four Cu atoms and 1 lone pair. No attractors corresponding to Cu−Cu interactions were found. The ELF distribution has minima at the lines connecting the Cu atoms (Figure 7G−J).

No drastic difference in the Cu−P2 interactions is detected by COHP analysis in contrast to the ELF results. While ELF calculations suggest the presence of multicenter bonds between the Cu and P atoms, this cannot be further elucidated with COHP, where the bonding character is only analyzed along the lines connecting two atoms. In addition, ELF calculations showed no attractors corresponding to Cu−Cu interactions, while COHP suggests weak interactions along a shorter Cu−Cu distance of 2.55 Å. This demonstrates the importance of a comprehensive approach toward analysis of chemical bonding in intermetallic compounds.

DSC of $LaCu_{1+x}P_2$. $LaCu_{1+x}P_2$ exhibits remarkable thermal stability under static vacuum (Figure 8). No melting or phase transitions were observed upon heating the sample in the evacuated and sealed silica ampule up to 1273 K. No extra impurity peaks were found in the DSC curve, which also confirms the high purity of the polycrystalline sample. The powder XRD pattern of the thermally analyzed sample is similar to the pattern of the pristine sample, thus indicating the high stability of $LaCu_{1+x}P_2$ (Figure S1 in the SI).

Transport Properties of $LaCu_{1+x}P_2$. Because only $LaCu_{1+x}P_2$ was produced as a single-phase material, transport properties were studied for this compound. The temperature-dependent resistivity of $LaCu_{1+x}P_2$ was measured in the temperature range of 2−300 K, and the heating and cooling curves lie on top of each other (Figure 9). The room

dx.doi.org/10.1021/ic502234w | Inorg. Chem. 2015, 54, 890−897

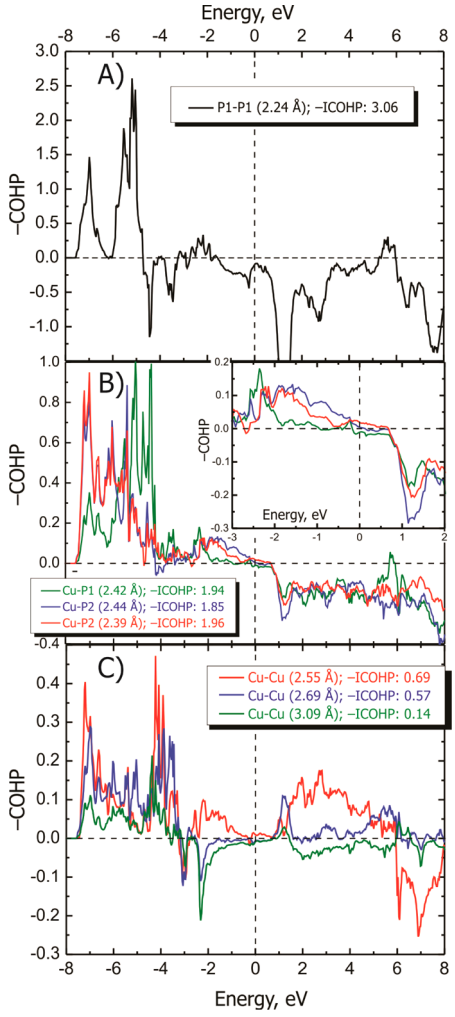

Figure 6. COHP plots for (A) P–P, (B) Cu–P, and (C) Cu–Cu interactions. ICOHP values (eV per bond) are given in the legend. The inset in part B shows an enlarged area near the Fermi level.

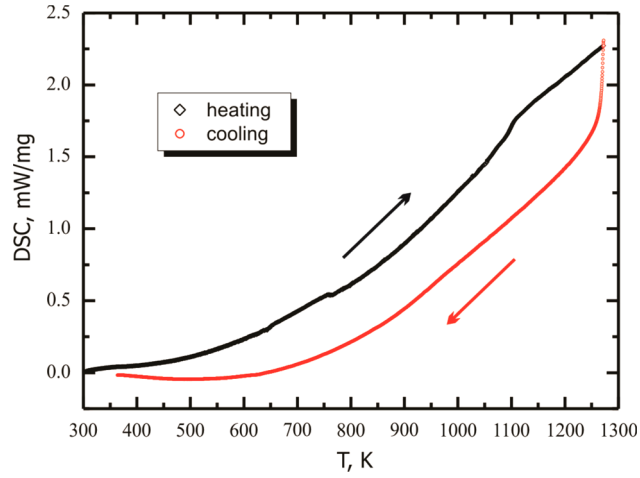

Figure 8. DSC profile for $LaCu_{1+x}P_2$.

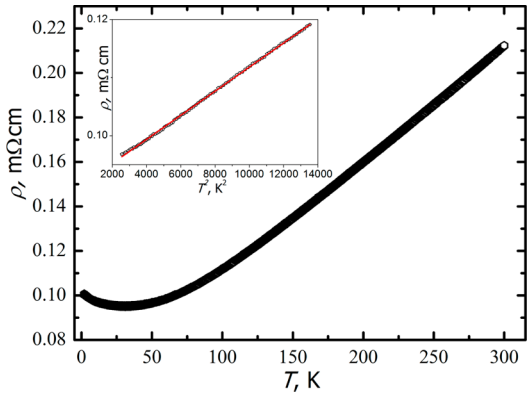

Figure 9. Temperature-dependent resistivity of $LaCu_{1+x}P_2$. The inset shows a linear fit of ρ versus T^2 (red line) in the range of 50–120 K.

temperature value of resistivity of 0.21 mΩ·cm is comparable with that of $La_5Cu_{19}P_{12}$ (0.35 mΩ·cm at 300 K).[17] With

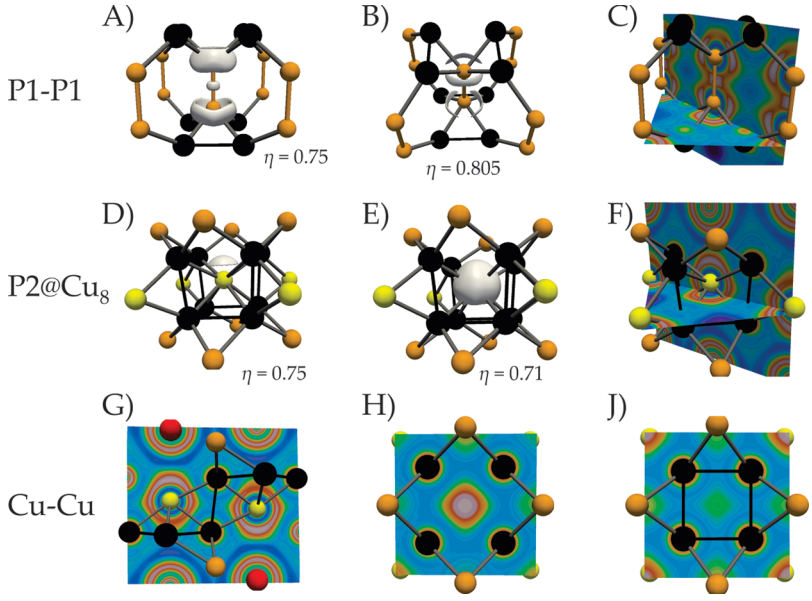

Figure 7. 3D isosurfaces (A, B, D, and E) and slices (C, F, G, H, and J) of the ELF η for $LaCu_4P_3$: (A–C) P1–P1 local coordination; (D–F) P2@Cu_8 trapezoidal prism; (G–J) Cu–Cu bonding with the shortest Cu–Cu distances (<2.7 Å) shown as black lines. Color code: La, red; Cu, black; P1, orange; P2, yellow.

dx.doi.org/10.1021/ic502234w | Inorg. Chem. 2015, 54, 890–897

increasing temperature, the resistivity first decreases from 2 to 35 K and then increases rapidly up to 300 K, which suggests a complex conduction mechanism. Such behavior is typical for an electronic phase transition from metal to semiconductor or from metal to semimetal. Other compounds demonstrating this type of low-temperature electronic behavior include CaMgSi,[52] $Sc_3B_{0.75}C_3$,[53] and Ba_3Si_4.[54] The inset in Figure 9 shows that the low-temperature resistivity in the range of 50−120 K depends linearly on T^2, indicating that the resistivity in this range is dominated by electron−electron interactions.[17]

As expected for the metallic compound, the Seebeck thermopower of $LaCu_{1+x}P_2$ is relatively low (Figure 10). The

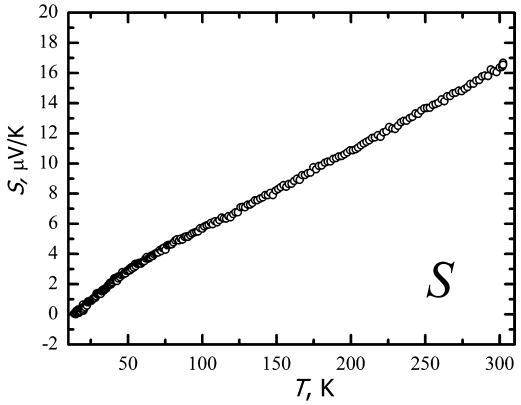

Figure 10. Temperature dependence of the Seebeck thermopower of $LaCu_{1+x}P_2$.

thermopower increases linearly within the whole temperature range, achieving 17 μV/K at room temperature. The thermopower is positive, indicating that holes are the main charge carriers. Despite the high electrical conductivity, the thermal conductivity of $LaCu_{1+x}P_2$ is quite small (Figure 11). The

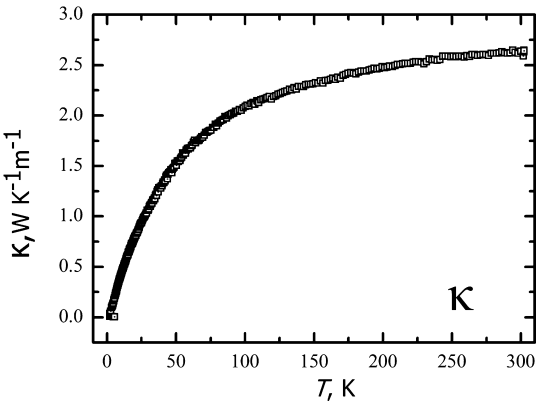

Figure 11. Temperature dependence of the thermal conductivity of $LaCu_{1+x}P_2$.

thermal conductivity rapidly increases from 2 to 50 K and increases more slowly, reaching 2.6 W/m·K at room temperature. Such a low value for a crystalline metallic conductor with a relatively small number of atoms in the unit cell and small atomic displacement parameters for all atoms may be explained by the structural disorder in the $Cu_{2x}P_2$ layers. Stacking of $Cu_{2x}P_2$ layers with different local order may introduce significant barriers for the propagation of heat-carrying phonons. Indeed, for crystalline disorder-free compounds, a pronounced maximum at ∼100 K is expected for temperature-dependent thermal conductivity.[55] $LaCu_{1+x}P_2$ exhibits no such maxima; instead, a gradual increase of the thermal conductivity is observed. This is typical for glasses and disordered crystalline solids.[55]

The calculated thermoelectric figure of merit, ZT, is 0.01 at 300 K. Investigations of the high-temperature thermoelectric properties as well as the effect of the copper concentration on the thermoelectric properties are currently underway.

CONCLUSIONS

The synthesis, crystal structure, chemical bonding, and transport properties of two new lanthanum copper phosphides, $LaCu_{1+x}P_2$ and $LaCu_4P_3$, are reported. Both compounds exhibit distortions of square-planar layers comprised of either P ($LaCu_{1+x}P_2$) or Cu ($LaCu_4P_3$) atoms. These distortions lead to unconventional multicenter Cu−P bonding in $LaCu_4P_3$, as revealed by ELF and COHP analyses. $LaCu_{1+x}P_2$ is a metallic-type conductor with high thermal stability. The presence of distorted P layers results in unexpectedly low values of thermal conductivity for $LaCu_{1+x}P_2$.

ASSOCIATED CONTENT

Supporting Information

CIF files, tables with crystallographic and EDS data, and figures of EDS spectra and powder XRD patterns. This material is available free of charge via the Internet at http://pubs.acs.org.

AUTHOR INFORMATION

Corresponding Author

*E-mail: kkovnir@ucdavis.edu. Phone: 1-530-752-5563.

Author Contributions

The manuscript was written through the contributions of all authors. All authors have given approval to the final version of the manuscript

Notes

The authors declare no competing financial interest.

ACKNOWLEDGMENTS

We thank Dr. A. V. Olenev (UC Davis) for help during the initial stage of this project and Prof. S. M. Kauzlarich (UC Davis) for access to the DSC and SPS. This research is supported by the U.S. Department of Energy, Office of Basic Energy Sciences, Division of Materials Sciences and Engineering, under Award DE-SC0008931. K.L. is thankful for the GAANN fellowship. Use of the APS at Argonne National Laboratory was supported by the U.S. Department of Energy, Office of Science, Office of Basic Energy Sciences, under Contract DE-AC02-06CH11357.

REFERENCES

(1) (a) Smetana, V.; Lin, Q.; Pratt, D. K.; Kreyssig, A.; Ramazanoglu, M.; Corbett, J. D.; Goldman, A. I.; Miller, G. J. *Angew. Chem., Int. Ed.* **2012**, *51*, 12699−12702. (b) Corbett, J. D. *Eur. J. Inorg. Chem.* **2011**, 3821−3822. (c) Corbett, J. D. *Inorg. Chem.* **2010**, *49*, 13−28. (d) Corbett, J. D. *Angew. Chem., Int. Ed.* **2000**, *39*, 670−690.

(2) Mills, A. M.; Lam, R.; Ferguson, M. J.; Deakin, L.; Mar, A. *Coord. Chem. Rev.* **2002**, *233*−*234*, 207−222.

(3) *Chemistry, Structure and Bonding of Zintl Phases and Ions*; Kauzlarich, S. M., Ed.; VCH Publishers: New York, 1996; and references cited therein.

(4) Papoian, G. A.; Hoffmann, R. *Angew. Chem., Int. Ed.* **2000**, *39*, 2408−2488.

(5) Cameron, J. M.; Hughes, R. W.; Zhao, Y.; Gregory, D. H. *Chem. Soc. Rev.* **2011**, *40*, 4099−4118.
(6) (a) Rotter, M.; Tegel, M.; Johrendt, D. *Phys. Rev. Lett.* **2008**, *101*, 107006. (b) Zheng, C.; Hoffmann, R. *J. Solid State Chem.* **1998**, *72*, 58−71. (c) Jia, S.; Williams, A. J.; Stephens, P. W.; Cava, R. J. *Phys. Rev. B* **2009**, *80*, 165107. (d) Jia, S.; Cava, R. J. *Phys. Rev. B* **2010**, *82*, 180410(R). (e) Jia, S.; Jiramongkolchai, P.; Suchomel, M. R.; Toby, B. H.; Checkelsky, J. G.; Ong, N. P.; Cava, R. J. *Nat. Phys.* **2011**, *7*, 207−210. (f) Han, J. T.; Zhou, J. S.; Cheng, J. G.; Goodenough, J. B. *J. Am. Chem. Soc.* **2013**, *132*, 908−909.
(7) (a) Kovnir, K.; Reiff, W. M.; Menushenkov, A. P.; Yaroslavtsev, A. A.; Chernikov, R. V.; Shatruk, M. *Chem. Mater.* **2011**, *23*, 3021−3024. (b) Thompson, C. M.; Kovnir, K.; Garlea, V. O.; Choi, E. S.; Zhou, H. D.; Shatruk, M. *J. Mater. Chem. C* **2014**, *2*, 7561−7569. (c) Kovnir, K.; Thompson, C. M.; Garlea, V. O.; Haskel, D.; Polyanskii, A. A.; Zhou, H. D.; Shatruk, M. *Phys. Rev. B* **2013**, *88*, 104429. (c) Kovnir, K.; Garlea, V. O.; Thompson, C. M.; Zhou, H. D.; Reiff, W. M.; Ozarowski, A.; Shatruk, M. *Inorg. Chem.* **2011**, *50*, 10274−10283. (d) Kovnir, K.; Thompson, C. M.; Zhou, H. D.; Wiebe, C. R.; Shatruk, M. *Chem. Mater.* **2010**, *22*, 1704−1713.
(8) Pralong, V.; Souza, D. C.; Leung, K. T.; Nazar, L. F. *Electrochem. Commun.* **2002**, *4*, 516−520.
(9) Gillot, F.; Boyanov, S.; Dupont, L.; Doublet, M.; Morcrette, M.; Monconduit, L.; Tarascon, J.-M. *Chem. Mater.* **2005**, *17*, 6327−6337.
(10) Monconduit, L. *J. Phys. Chem. C* **2014**, *118*, 10531−10544.
(11) Fulmer, J.; Lebedev, O. I.; Roddatis, V. V.; Kaseman, D. C.; Sen, S.; Dolyniuk, J.; Lee, K.; Olenev, A. V.; Kovnir, K. *J. Am. Chem. Soc.* **2013**, *135*, 12313−12323.
(12) Fulmer, J.; Kaseman, D. C.; Dolyniuk, J.; Lee, K.; Sen, S.; Kovnir, K. *Inorg. Chem.* **2013**, *52*, 7061−7067.
(13) Dolyniuk, J.; Kaseman, D. C.; Sabyasachi, S.; Zhao, J.; Osterloh, F. E.; Kovnir, K. *Chem.—Eur. J.* **2014**, *20*, 10829−10837.
(14) Lee, K.; Synnestvedt, S.; Bellard, M.; Kovnir, K. *J. Solid State Chem.* **2014**, DOI: 10.1016/j.jssc.2014.04.021.
(15) Chikhrii, S. I.; Kuz'ma, Y. B.; Orishchin, S. V. *Dopov. Akad. Nauk Ukr. RSR, Ser. B: Geol., Khim. Biol. Nauki* **1989**, *3*, 60−62.
(16) Chihrii, S. I. *Russ. J. Inorg. Chem.* **1990**, *35*, 942−944.
(17) Cava, R. J.; Siegrist, T.; Carter, S. A.; Krajewski, J. J.; Peck, W. F., Jr.; Zandbergen, H. W. *J. Solid State Chem.* **1996**, *121*, 51−55.
(18) Chikhrii, S. I.; Loukasouk, G. V.; Orishchin, S. V.; Kuz'ma, Y. B. *J. Alloys Compd.* **1997**, *248*, 224−232.
(19) Düenner, J.; Mewis, A. *Z. Anorg. Allg. Chem.* **1997**, *623*, 608−612.
(20) Kuz'ma, Y. B.; Chikhrii, S. I.; Mozharivsky, Y. A.; Tremel, W.; Demchyna, R. O. *J. Alloys Compd.* **1998**, *278*, 169−174.
(21) Mozharivsky, Y.; Kaczorowski, D.; Franzen, H. F. *J. Solid State Chem.* **2000**, *155*, 259−272.
(22) Mozharivsky, Y.; Kuz'ma, Y. B. *J. Solid State Chem.* **2000**, *151*, 150−156.
(23) Demchyna, R. O.; Orishchin, S. V.; Kuz'ma, Y. B. *J. Alloys Compd.* **2001**, *322*, 176−183.
(24) Mozharivsky, Y.; Pecharskii, V. K.; Franzen, H. F. *J. Alloys Compd.* **2002**, *345*, 100−104.
(25) Mozharivsky, Y.; Kaczorowski, D.; Franzen, H. F. *Z. Anorg. Allg. Chem.* **2001**, *627*, 2163−2172.
(26) Mozharivsky, Y.; Pecharsky, A. O.; Bud'ko, S. L.; Franzen, H. F. *Z. Anorg. Allg. Chem.* **2002**, *628*, 1619−1630.
(27) *APEX-II*; Bruker AXS Inc.: Madison, WI, 2005.
(28) Sheldrick, G. M. *Acta Crystallogr., Sect. A* **2008**, *A64*, 112−122.
(29) Jepsen, O.; Burkhardt, A.; Andersen, O. K. *The Program TB-LMTO-ASA*, version 4.7; Max-Planck-Institut für Festkörperforschung: Stuttgart, Germany, 1999.
(30) Dronskowski, R.; Blöchl, P. E. *J. Phys. Chem.* **1993**, *97*, 8617−8624.
(31) Becke, A. D.; Edgecombe, K. E. *J. Chem. Phys.* **1990**, *92*, 5397−5403.
(32) Savin, A.; Jepsen, O.; Flad, J.; Andersen, O. K.; Preuss, H.; Von Schnering, H. G. *Angew. Chem.* **1992**, *104*, 186−188; *Angew. Chem., Int. Ed. Engl.* **1992**, *31*, 187−188.
(33) Savin, A.; Nesper, R.; Wengert, S.; Fassler, T. F. *Angew. Chem.* **1997**, *109*, 1892−1918; *Angew. Chem., Int. Ed. Engl.* **1997**, *36*, 1808−1832.
(34) *Paraview: Parallel visualization application*, version 4.1.0 64 bit; Sandia National Labs, Kitware Inc., and Los Alamos National Labs, 2014; http://paraview.org.
(35) Baranov, A. I. *Visualization plugin for ParaView*, version 4.1.0; Springer: Berlin, 2014.
(36) *Inorganic Crystal Structure Database (ICSD)*, version 1.9.3; Fachinformationszentrum Karlsruhe: Karlsruhe, Germany, 2013.
(37) Keimes, V.; Johrendt, D.; Mewis, A. *Z. Anorg. Allg. Chem.* **1995**, *621*, 925−930.
(38) Jeitschko, W.; Foecker, A. J.; Paschke, D.; Dewalsky, M. V.; Evers, B. H.; Küennen, B.; Lang, A.; Kotzyba, G.; Rodewald, U. C.; Möeller, M. H. *Z. Anorg. Allg. Chem.* **2000**, *626*, 1112−1120.
(39) (a) Von Schnering, H. G.; Hönle, W. *Chem. Rev.* **1988**, *88*, 243−273. (b) Pöttgen, R.; Hönle, W.; Von Schnering, H. G. In *Encyclopedia of Inorganic Chemistry*, 2nd ed.; King, R. B., Ed.; Wiley: Chichester, U.K., 2005; Vol. *8*, pp 4255−4308. (c) Dolyniuk, J.; Kovnir, K. *Crystals* **2013**, *3*, 431−442. (d) Shatruk, M. M.; Kovnir, K.; Shevelkov, A. V.; Popovkin, B. A. *Angew. Chem., Int. Ed.* **2000**, *39*, 2508−2509.
(40) Ono, S.; Nomura, K.; Hayakawa, H. *J. Less-Common Met.* **1974**, *38*, 119−130.
(41) (a) Dünner, J.; Mewis, A. *Z. Anorg. Allg. Chem.* **1991**, *621*, 191−196. (b) Kovnir, K.; Stockert, U.; Budnyk, S.; Prots, Y.; Baitinger, M.; Paschen, S.; Shevelkov, A. V.; Grin, Y. *Inorg. Chem.* **2011**, *50*, 10387−10396.
(42) Chen, X.; Zhu, L.-P.; Yamanaka, S. *J. Solid State Chem.* **2003**, *173*, 449−455.
(43) Von Schnering, H. G.; Wichelhaus, W.; Schulze Nahrup, M. *Z. Anorg. Allg. Chem.* **1975**, *412*, 193−201.
(44) Chikhrii, S. I.; Orishchin, S. V.; Kuz'ma, Y. B. *Russ. J. Inorg. Chem.* **1987**, *32*, 1386−1388.
(45) Lincke, H.; Nilges, T.; Johrendt, D.; Poettgen, R. *Solid State Sci.* **2008**, *10*, 1006−1011.
(46) Brown, D. B.; Zubieta, J.; Vella, P. A.; Wrobleski, J. T.; Watt, T.; Hatfield, W. E.; Day, P. *Inorg. Chem.* **1980**, *19*, 1945−1950.
(47) He, H.; Tyson, C.; Bobev, S. *Inorg. Chem.* **2011**, *50*, 8375−8383.
(48) Charkin, D. O.; Urmanov, A. V.; Kazakov, S. M.; Batuk, D.; Abakumov, A. M.; Knöner, S.; Gati, E.; Wolf, B.; Lang, M.; Shevelkov, A. V.; Tendeloo, G. V.; Antipov, E. V. *Inorg. Chem.* **2012**, *51*, 8948−8955.
(49) (a) Olofsson, O. *Acta Chem. Scand.* **1965**, *19*, 229−241. (b) Moeller, M. H.; Jeitschko, W. *Z. Anorg. Allg. Chem.* **1982**, *491*, 225−236. (c) Lange, S.; Bawohl, M.; Weihrich, R.; Nilges, T. *Angew. Chem., Int. Ed.* **2008**, *47*, 5654−5657.
(50) Wen, X. D.; Cahill, T. J.; Hoffmann, R. *J. Am. Chem. Soc.* **2009**, *131*, 2199−2207.
(51) Cuervo-Reyes, E.; Nesper, R. *Phys. Rev. B* **2014**, *90*, 064416.
(52) Whalen, J. B.; Zaikina, J. V.; Achey, R.; Stillwell, R.; Zhou, H. D.; Wiebe, C. R.; Latturner, S. E. *Chem. Mater.* **2010**, *22*, 1846−1853.
(53) Mori, T.; Shi, Y.; Tanaka, T. *J. Alloys Compd.* **2000**, *308*, 115−120.
(54) Aydemir, U.; Ormeci, A.; Borrmann, H.; Boehme, B.; Zuercher, F.; Uslu, B.; Goebel, T.; Schnelle, W.; Simon, P.; Carrillo Cabrera, W.; Haarmann, F.; Baitinger, M.; Nesper, R.; Von Schnering, H. G.; Grin, Y. *Z. Anorg. Allg. Chem.* **2008**, *634*, 1651−1661.
(55) (a) *CRC Handbook of Thermoelectrics*; Rowe, D. M., Ed.; CRC: Boca Raton, FL, 1995. (b) Kittel, C. *Introduction to Solid State Physics*, 8th ed.; Wiley: New York, 2004.